Sensors and Actuators B 265 (2018) 660–667

Contents lists available at ScienceDirect

Sensors and Actuators B: Chemical

journal homepage: www.elsevier.com/locate/snb

Fully integrated and portable semiconductor-type multi-gas sensing module for IoT applications

Ji-Hoon Suh [a], Incheol Cho [a], Kyungnam Kang [a], Soon-Jae Kweon [b], Moonjin Lee [c], Hyung-Joun Yoo [b], Inkyu Park [a,*]

[a] Department of Mechanical Engineering, KAIST, Daejeon, 34141, Republic of Korea
[b] School of Electrical Engineering, KAIST, Daejeon, 34141, Republic of Korea
[c] Korea Research Institute of Ships & Ocean Engineering, Daejeon, 34103, Republic of Korea

ARTICLE INFO

Article history:
Received 1 November 2017
Received in revised form 1 February 2018
Accepted 16 March 2018
Available online 19 March 2018

Keywords:
Constant power
Gas sensor array
Interface circuit
IoT
Semiconductor gas sensor
Wide-range resistacnce readout

ABSTRACT

This paper suggests a portable multi-gas sensing module with chemiresistive gas sensors on a micro-electro-mechanical-systems (MEMS)-based heating platform. MEMS gas sensors are composed of four microheaters mounting heterogeneous sensing nanomaterials (SnO_2 nanotubes and ZnO nanowires with/without a Pt catalyst) and operating power is only 6 mW per each heater. A comprehensive approach to control heaters and readout multiple resistive sensors is implemented on a printed circuit board through the combination of analog/digital signal processing and a highly reconfigurable circuit structure. A wide range of sensor resistance (1 kΩ-100 MΩ) can be read with a relative error less than 1% by adaptively adjusting the gain of a trans-impedance amplifier. Heater controller circuits are operated in a way to give optimized power for each heater, and the target power is maintained at a constant value to keep a stable temperature condition. The module's multiple gas sensing capability enables selectivity enhancement by principle component analysis (PCA). Operation mode is readily reprogrammed to give repetitive sleep mode, and it is demonstrated that fabricated sensors show decent response and recovery to frequent heater on/off repetition. For both of portable and stationary applications, Bluetooth Low Energy and Wi-Fi communication is realized through a RF-microcontroller combination system-on-chip (SoC).

1. Introduction

Gas monitoring systems are used in diverse fields from personal applications to industries, particularly for environmental monitoring or toxic gas detection. Recently, strong interests in the Internet of Thing (IoT) is drawing attention to small-sized and portable gas monitoring devices. In this point, semiconductor-type resistive gas sensors are very attractive due to their small size and high sensitivity. They are also easily produced, and have low cost. These advantages show that the semiconductor-type gas sensor is a good candidate for the IoT application. However, there are several hurdles that still obstruct the actual utilization of gas sensing systems based on these sensors: heaters tend to consume high power for battery-powered systems, and resistive type sensors have poor selectivity. In order to resolve this problem, we have previously suggested a highly integrated platform that enables multi-sensing in a micro-scale, consuming fairly low power around 6 mW [1]. Also, selectivity-enhancing techniques using multiple resistive sensors are being developed [2]. For circuit issues to interface the sensors, it needs to readout the resistance over a wide range (i.e. variation in several decades) [3], and heater drivers should provide constant power for sensors to maintain a controlled and optimized temperature. Many studies on the interface circuits suggest methods to overcome the aforementioned issues using stable DC-excitation [4] or pulse-width-modulation (PWM) schemes [5]. Among approaches that interface multichannel MEMS type sensors, resistance readout circuits using current-driving method was also proposed [6]. Despite those endeavors, implementation of on-board multiple gas sensing module appropriate for IoT is still difficult because of both the sensor and circuit issues.

This paper suggests a portable gas sensing module with an ultra-compact MEMS gas sensor device towards IoT application including multiple gas sensor readout and data analysis, analog/digital signal processing, heater control, and wireless communication. A DC-excitation method by trans-impedance amplifier (TIA) is used rather than PWM technique for more stable operation, avoiding sensor lifetime issue, and AC-affecting parasitic effects [3]. The gain-adjustable TIA enables wide range readout of sensor resis-

* Corresponding author.
E-mail address: inkyu@kaist.ac.kr (I. Park).

https://doi.org/10.1016/j.snb.2018.03.099
0925-4005/

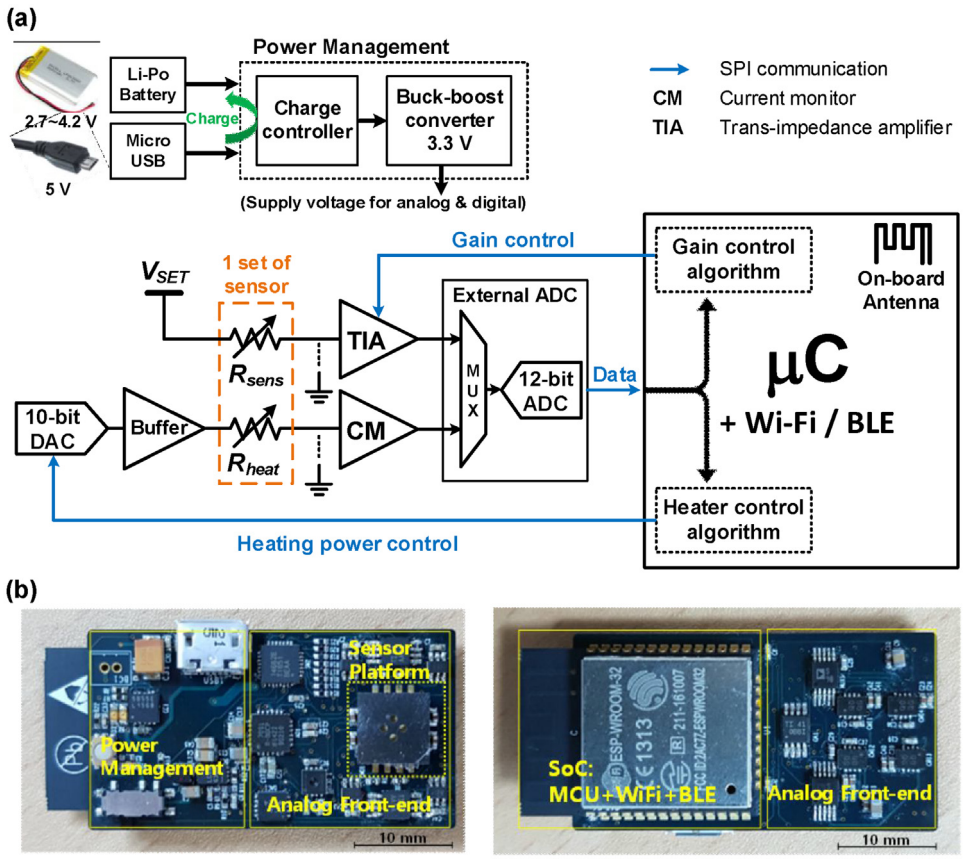

Fig. 1. (a) Simplified overview of the proposed system: power management part that provides stable power to the entire system, AFE to drive heaters and readout sensor signals, and microcontroller-RF combined SoC that controls the AFE components and transmit sensor data wirelessly. (b) Photo of front/back side of the sensor module.

tance, and digitally controllable heater driver makes highly flexible power injection for heaters. The use of a system-on-chip (SoC) chipset that incorporates a microprocessor and two wireless communication standards (Bluetooth Low Energy and Wi-Fi) achieves smaller size for the entire module and largely extend its possible applications for both stationary and portable uses. Also, it is demonstrated that poor selectivity issue in using a single metal-oxide gas sensor can be addressed when multiplexing a sensor array and conducting a principle component analysis (PCA).

In terms of fully integrated module design, our system is more accurate, size-efficient and has multiple sensor interfacing capability with wider sensing range at the same time as compared to previous works [7–9]. Although the integrated circuit (IC) design approaches [3–5] show higher performance, smaller size, and better versatility, our work is dedicated to designing a directly applicable end-to-end system toward IoT that those ICs have not yet supported. We achieved higher or comparable results to the IC approaches in the sensing range, accuracy, and capability of heater control while not sacrificing the portability of the module.

2. Interface circuits and module operation

2.1. Overview of the proposed system

The proposed gas sensing system mainly consists of three parts: power management part that provides stable power to the entire system, analog front-end (AFE) to drive heaters and readout sensor signals, and microcontroller-RF combined SoC that controls the AFE components and transmit sensor data wirelessly (Fig. 1). To begin with the power management part, this system can be powered by either a 5 V USB power source or a lithium-polymer battery with a nominal output voltage of 3.7 V. For the lithium-polymer batteries, their output normally varies from 4.2 V to 2.7 V over usage, while supply voltage of the whole system is 3.3 V. To ensure the system to operate even when battery output decreases under 3.3 V, a buck-boost converter is adopted. For this system, this type of power converter is more adequate for its conversion efficiency than other converters such as low-drop out (LDO) regulators. With a battery connected, the charge controller IC (LM3658, TI, USA) manages battery charging operation. When the system is powered by USB, the charge controller operates in LDO mode which generates constant 4.2 V. This voltage is then converted to 3.3 V through the buck-boost converter.

The AFE excites resistive gas sensors (R_{sens}) and controls power to the heaters (R_{heat}). A constant voltage is applied to R_{sens} so that it gives current which corresponds to the resistance. For R_{heat}, a digital-to-analog converter (DAC)–AD5314, Analog Devices, USA–is adopted for flexible power control through the microcontroller, and the current through the R_{heat} is monitored using a current monitoring chip, which facilitates power monitoring.

The microcontroller-RF combined SoC (ESP32, Espressif Systems, China) receives data from the sensors through an external analog-to-digital converter (ADC)–AD7091R-8, Analog Devices, USA. This sensing data is transmitted through either Bluetooth Low Energy (BLE) or Wi-Fi. Also, software-based algorithm is implemented for the gain control of the TIA and heater power control. The whole module has the size of 44×21 mm^2.

2.2. Circuit details of AFE for sensors and heaters

As shown in Fig. 2(a), R_{sens} is excited by a DC voltage, and the resistance data is converted to the current. The TIA with vari-

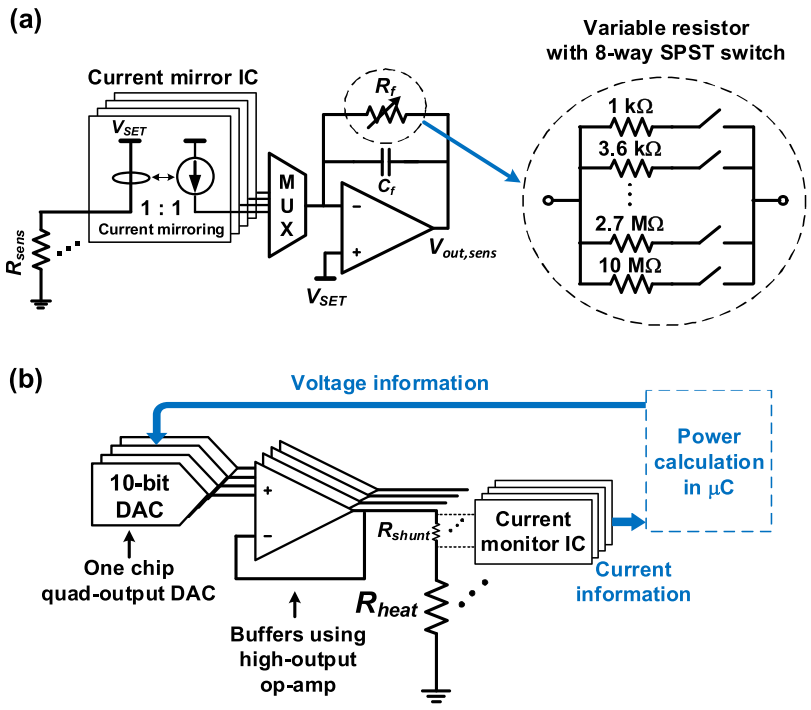

Fig. 2. (a) Interface circuit for R_{sens} and implementation of variable R_f. R_{sens} is excited by a DC voltage and the resistance data is converted to the current. Current mirrors are adopted to isolate TIAs from a MUX switching effect. (b) DAC-based heater driving and power monitoring circuits with current monitoring scheme over a shunt resistor. High-output buffers are adopted to overcome the DAC output power limitations.

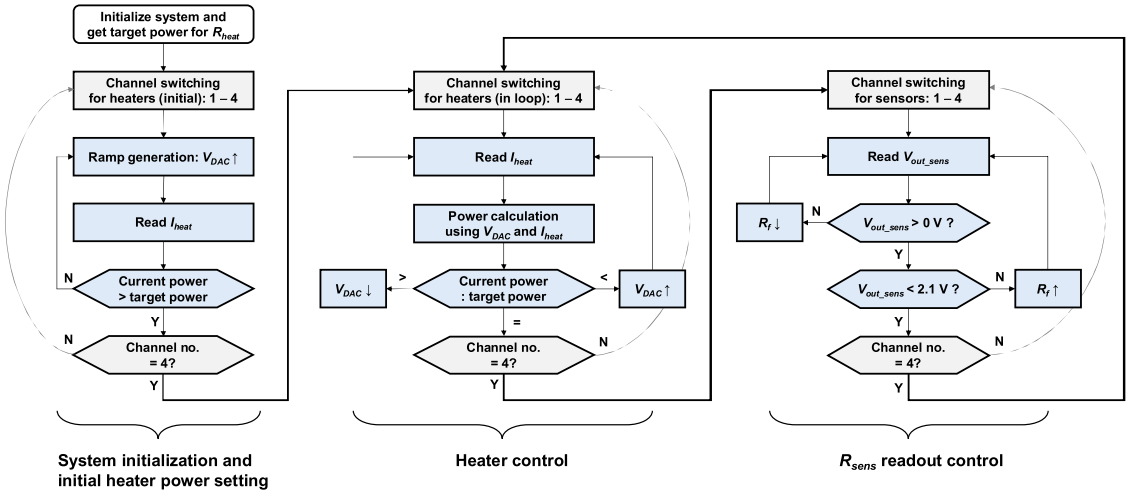

Fig. 3. Simplified schematic of algorithm programmed in the microprocessor (ESP32). In the first process, circuit components in AFE are initialized and each heating power is initially set to the target value by generating a ramp voltage (V_{DAC}). For the heater control, heating power is maintained at the target value by monitoring I_{heat} and then adjusting V_{DAC}. For the R_{sens} readout control, appropriate R_f is automatically selected in a way to avoid the saturation of the TIA output.

able gain by R_f then converts it to the voltage in order to make it readable by the ADC. Multiple R_{sens} shares one variable-gain TIA because the circuit takes large volume on the module. Here, a wide-range (3 nA–3 mA) logarithmic current mirror IC (ADL5315, Analog Devices, USA) is adopted. It allows user-definable voltage application (V_{SET}) as high as possible to make the resultant current more sensitive to R_{sens}, and to keep R_{sens} from unnecessary switching effect from the multiplexer so that it maintains stable DC-excitation condition even during the switching of MUX. Since the accuracy of current mirror is at the best when the output node voltage is the same with V_{SET} (2.3 V), the reference voltage for TIA is chosen to be the same as V_{SET} (positive terminal of the op-amp). R_f determines the conversion gain from the current to the voltage, and it is set to cover a wide range of R_{sens} variation. This is because the resistance change in the resistive gas sensors is usually very large [3], and it also should cover diversified resistance over multiple input channels. Therefore, the variable R_f consists of a set of resistors with switches connected to each of them. The resistors are an array of commercial chip resistors ranging from 1 kΩ to 10 MΩ with an interval slightly more than a half decade (1 kΩ, 3.6 kΩ, 13 kΩ, 51 kΩ, 180 kΩ, 760 kΩ, 2.7 MΩ, and 10 MΩ). Taking into account the sensor driving voltage and reference voltage (V_{SET}), the V_{out} is as follows

$$V_{out} = V_{SET}\left(1 - \frac{R_f}{R_{sens}}\right). \quad (1)$$

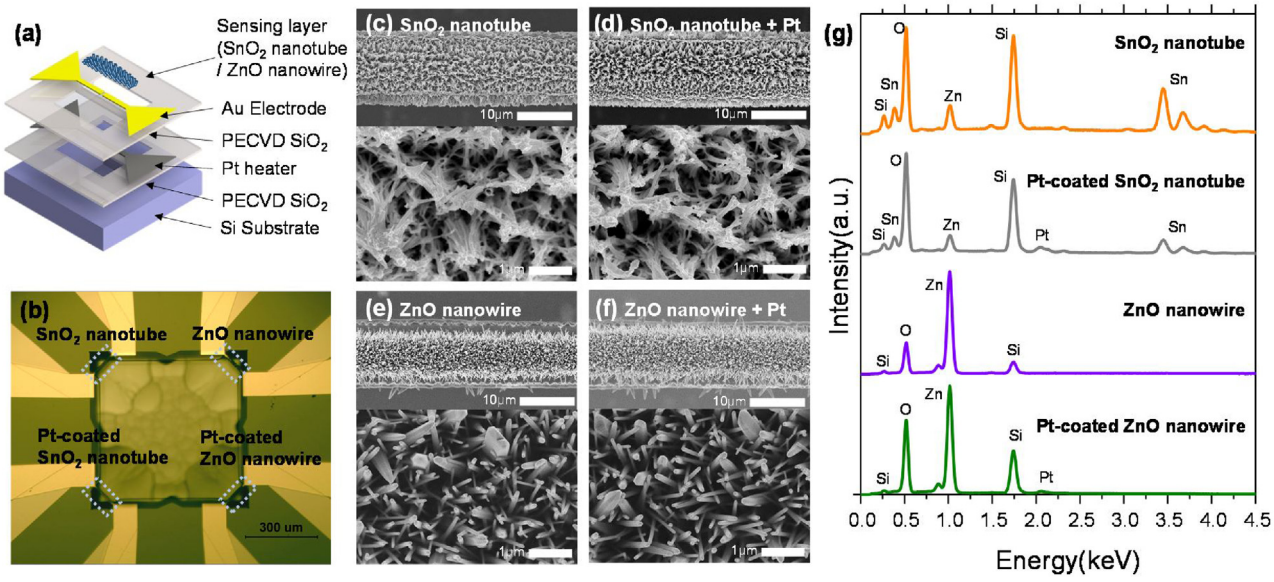

Fig. 4. (a) Schematic of a low power MEMS gas sensor; (b) A 2 × 2 sensor array composed of heterogeneous metal oxide nanomaterials (i.e. SnO_2 nanotubes, Pt-coated SnO_2 nanotubes, ZnO nanowires and Pt-coated ZnO nanowires) on a single chip; their (c-f) SEM images and (g) EDS spectra.

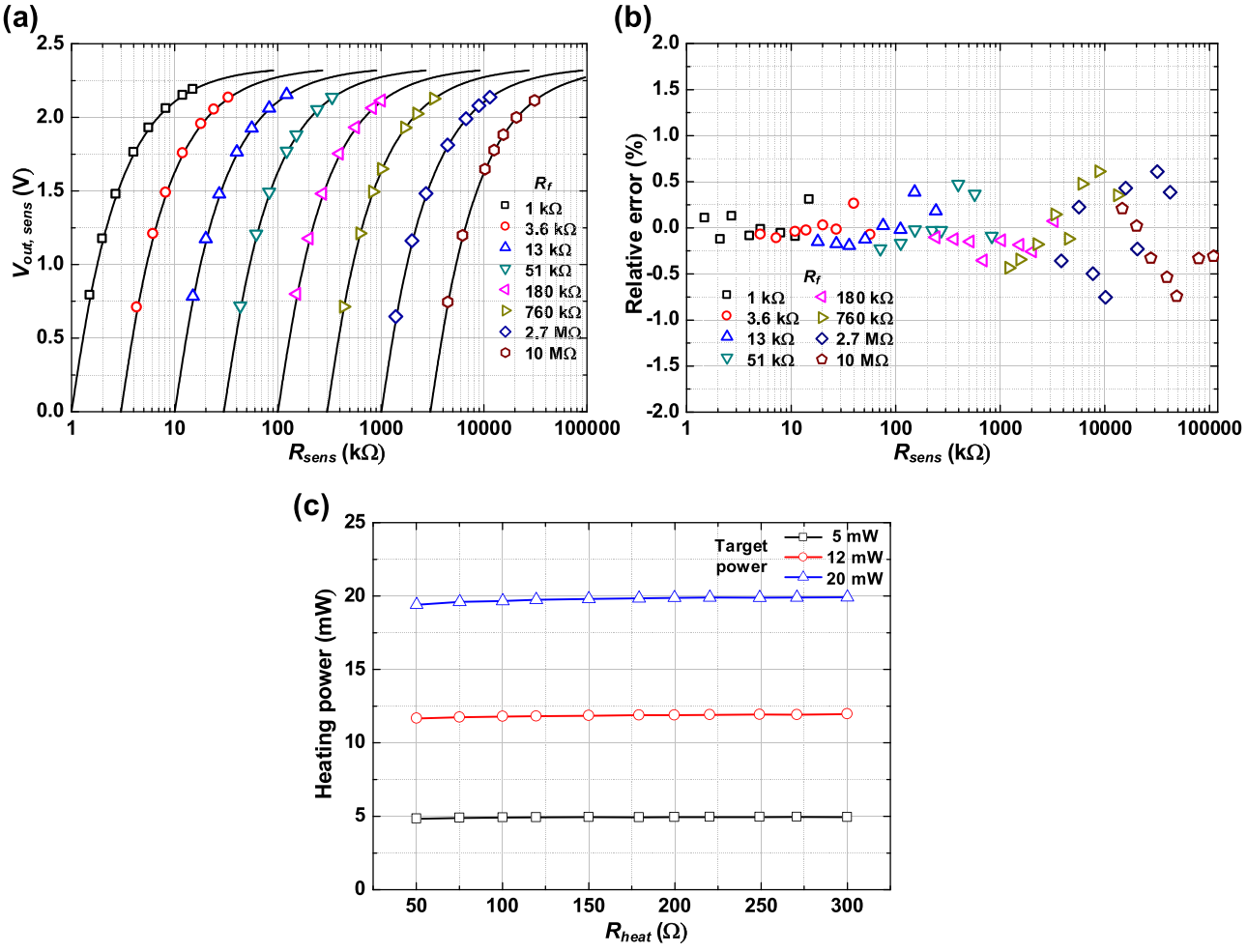

Fig. 5. (a) Output voltages of R_f-adjustable TIA according to the change of R_{sens}. A wide range of R_{sens} is covered due to a wide possible range of R_f. (b) Relative error of R_{sens} from the ideal values. For the given range of R_{sens}, the error is less than 1%. (c) Constant power application by three different target powers according to the variation of R_{heat}.

Considering the reference voltage of the TIA (2.3 V), readable R_{sens} range is roughly from 1 kΩ to 100 MΩ. Low on-resistance, 8-way single-pole single-through (SPST) IC switch (MAX14662, Maxim Integrated, USA) is utilized to make it digitally controllable. This switch is appropriate even with high R_{sens} (in the order of MΩ) that will result in the hundreds of nA through the TIA, because

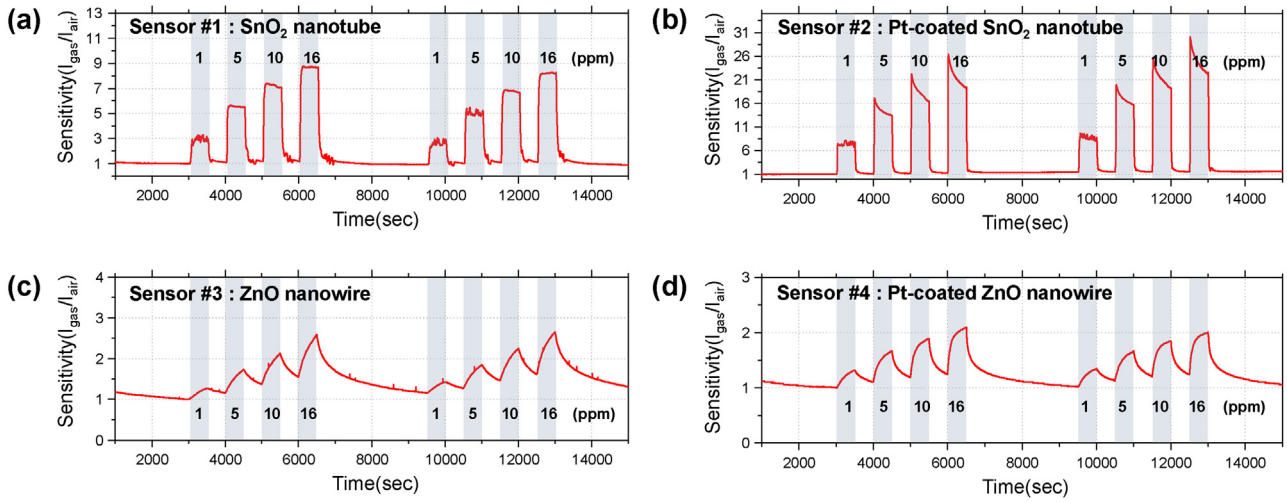

Fig. 6. Experimental results of the gas sensing module for four different concentrations of H_2S. (a) Bare SnO_2 nanotube, (b) Pt-coated SnO_2 nanotube with enhanced sensitivity, (c) Bare ZnO nanowire, and (d) Pt-coated ZnO nanowire with enhanced sensitivity; In general, SnO_2-based nanotubes have better performances than ZnO nanowires in the response/recovery speed and sensitivity.

it has very small leakage current no more than 1 nA within the operation range. For the same reason, low leakage MUX (ADG704, Analog Devices, USA) and the op-amp with pA-ordered input bias current are chosen (OPA2376, TI, USA). The MUX has a low on-resistance (<4 Ω) and the op-amp is a precision type with rail-to-rail input/output.

2.3. Heater control

Since each kind of gas sensors has its own optimal temperature to operate and the temperature can be changed by external effects such as cooling, it is necessary for the heating power to be constantly monitored and controlled. For this necessity, a real-time heater control is implemented. Fig. 2(b) shows the heater driving and power monitoring circuits with current monitoring scheme over a shunt resistor. The use of DAC allows to readily control power using a microcontroller without the need to measure the heater voltage. For the DAC, 10-bit, 4-channel DAC (AD5314, Analog Devices, USA) is adopted. Here, lack of high-current driving capability of DAC necessitates a high-output power op-amp. Therefore, precision, rail-to-rail, and high-output type op-amp (LM7332, TI, USA) is used. Since relatively high current (around 10 mA) is drawn by R_{heat}, the gain for current monitoring IC is chosen to be as low as 100 V/V. A burden voltage across R_{shunt} is unavoidable, and is 1 mV/mA in this system. This effect is calibrated by software for the power calculation. For the current readout resolution, it is theoretically 12 μA when considering the current monitor's gain (100 V/V) and 12-bit ADC with 2.5 V reference. The output of the current monitoring is read through the ADC, and the power is constantly calculated based on DAC value and measured current. This enables customized and constant power injection to the heaters, providing a stable temperature condition for the gas sensors.

2.4. Microprocessor operation

Fig. 3 is the simplified schematic of the algorithm programmed in the microprocessor (ESP32). When the system starts, various initialization for AFE circuit components is first conducted and the heater power reaches its target power by generating a ramp voltage (V_{DAC}). For the heater control algorithm, current flowing through the heater (I_{heat}) is monitored so that the microprocessor can calculate the power, and maintain it at the target by adjusting V_{DAC}. In order to read R_{sens} in real time, R_f should be automatically selected to avoid the saturation of TIA output voltage (V_{out_sens}). If V_{out_sens} approaches to 0 V, lower R_f is chosen. For the opposite case, 2.1 V is chosen to be the upper limitation to change R_f. This is because, if V_{out_sens} approaches to the TIA reference (i.e. 2.3 V), even a very small noise on V_{out_sens} may cause a large error in the calculation of R_{sens}. This situation can be found in the ideal lines of Fig. 5(a), where small discrepancy of measured V_{out_sens} may cause large error in R_{sens} as the lines get close to 2.3 V.

3. Low power MEMS gas sensor array: fabrication and characterization

In our previous report, we introduced a MEMS-based low power microheater platform [10–14], in which each heater is configured as a suspended dual-cantilever structure in order to minimize the thermal power consumption (Fig. S1 in the Supplementary Information). The beam-shaped suspended microheater has 9 μm in width and 110 μm in length. Microheaters were fabricated through conventional MEMS processes such as UV-photolithography, chemical vapor deposition (CVD), electron beam (e-beam) evaporation, and silicon wet etching, etc. Because of the microscale size of the heating area, the power needed to rise the temperature to 260 °C was only 6 mW. On a single chip, a 2 × 2 array of microheaters was integrated.

A localized hydrothermal synthesis and liquid-phase deposition (LPD) process were used to effectively integrate the sensing nanomaterials into a small heating spot. The fabrication process consists of the following four steps: (1) a pair of the microheaters was heated at 45 mW (~95 °C) for 15 min in an aqueous ZnO precursor (25 mM of zinc nitrate hydrate, 25 mM of hexamethylenetetramine (HMTA), and 6 mM of polyethyleneimine (PEI) in DI water, all chemicals were purchased from Sigma Aldrich). (2) Then, synthesized ZnO nanowires were put into a SnO_2 LPD solution (3.75 mM SnF_2, 15 mM of HF, 7.5 mM of H_2O_2, and 37.5 mM of H_3BO_3 in DI water) and substituted with SnO_2 nanotubes for 20 min. (3) ZnO nanowires were grown on the other pair of the bare microheater through the same method as step (1). (4) A pair of microheaters containing the synthesized ZnO nanowires and SnO_2 nanotubes was covered with a shadow mask, and the remaining pair was coated with Pt nanoparticles using electron beam evaporation (thickness of Pt ~ 2 nm). As a result, a sensor array consisting of bare SnO_2 nanotubes, Pt-coated SnO_2 nanotubes, bare ZnO nanowires, and Pt-coated ZnO nanowires could be fabricated (Fig. 4(b)).

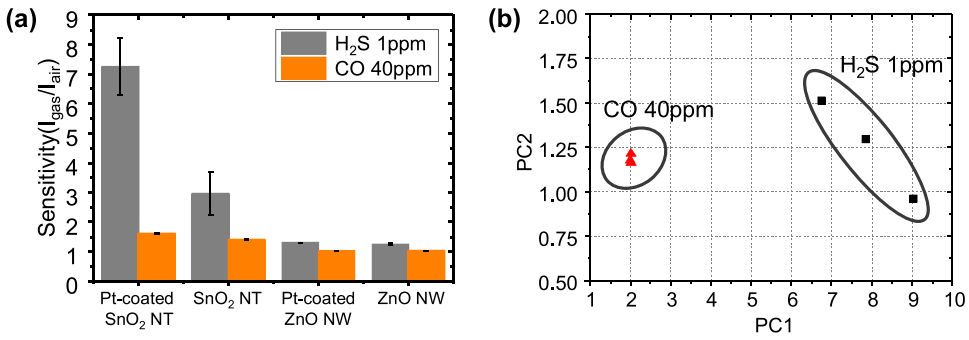

Fig. 7. Sensitivity analysis of the sensor array for the enhancement of gas selectivity. (a) Sensitivity comparison of the sensor array to H_2S and CO gases, and (b) PCA result based on the acquired sensitivity. Sufficiently distinct distribution of the sets of points in PCA allows the sensing system to distinguish these two gases.

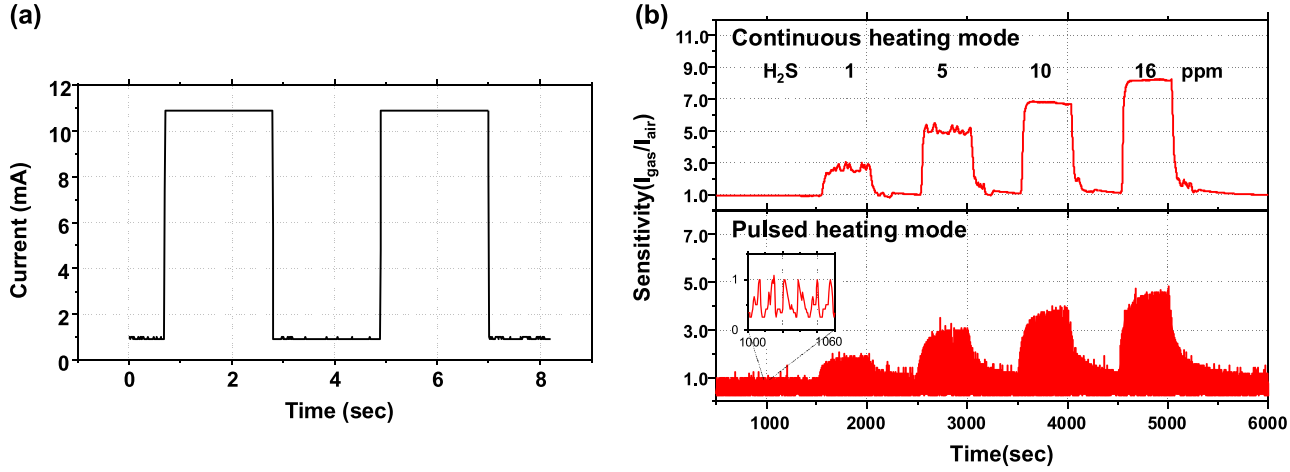

Fig. 8. Sensor responses in a pulse-heating condition. (a) The resultant pulse current into a heater by a pulse voltage and (b) comparison of H_2S gas responses between continuous and pulse heating modes. Even though sensitivity and response/recovery speed are reduced compared to the continuous heating condition, the sensor still gives fair gas response and recovery/response in the pulse-heating mode.

SEM and SEM-energy dispersive spectroscopy (EDS) analysis were carried out for the characterization of fabricated sensor arrays. Fig. 4(c–f) show the SEM images of bare SnO_2 nanotubes, Pt-coated SnO_2 nanotubes, bare ZnO nanowires, and Pt-coated ZnO nanowires, respectively. The average diameter and length of the ZnO nanowires are about 70 nm and 1 μm, respectively, and form a complex electrical network due to their random growing direction (Fig. 4(e–f)). In addition, due to the acidic condition of the LPD solution, ZnO nanowires were dissolved and a hollow structure of SnO_2 nanotubes was formed (Fig. 4(c–d)). Fig. 4(g) shows the EDS spectra of the synthesized nanomaterials. The Pt peaks were clearly observed in Pt-coated SnO_2 nanotubes/ZnO nanowires, while no Pt peaks were observed in bare SnO_2 nanotubes/ZnO nanowires that were shaded by the shadow mask during e-beam evaporation process.

4. Results and discussion

4.1. Measurement results of the module

Fig. 5(a) shows the output voltages of the TIA for each R_f over a wide input range of R_{sens}. Since the output voltage is mainly determined by the ratio of R_f and R_{sens} as Eq. (1) shows, larger R_f enables to cover wider range of R_{sens} variation. The measured points well follow the solid lines which represent ideal curves drawn using Eq. (1). Based on the measured V_{out_sens}, R_{sens} is calculated by the microcontroller, and relative error from the ideal values are shown in Fig. 5(b). Although the relative error tends to get larger as R_{sens} increases because it gets more susceptible to noise and leakage, it is still less than 1%. To maintain appropriate temperatures for sensors, heating power should be maintained regardless of variation in R_{heat}. Fig. 5(c) shows that for randomly chosen three cases of target power applied for the heaters (5, 12, 20 mW), the control algorithm inside the microcontroller enables the application of the target power and make the power constant regardless of the change of R_{heat}. This experiment is to show the capability of pure circuits and algorithms for power control. Therefore, instead of using fabricated microheaters for R_{heat}, we utilized commercially available fixed carbon film resistors, whose resistances are not sensitive to temperature (<100 ppm/°C).

4.2. Measurement results of module with sensor array

Fig. 6 shows four-channel real-time plots of the sensor responses to H_2S gas that are acquired by the module. We observed that the wide range of resistances were covered for all channels (current from nA-order to the hundreds of μA at V_{SET}) with heating power maintained at 6 mW for each heater, producing temperature around 260 °C (Fig. S2 in the Supplementary Information). Cyclic on-off period of H_2S gas was 500 s, and the concentration of H_2S ranged in 1–16 ppm. The sensors responded to H_2S with different sensitivities and response speeds while SnO_2 nanotubes showed better performances. In Fig. 6(b), the highest sensitivity was obtained for the Pt-coated SnO_2 nanotubes (I_{gas}/I_{air} = 8.5 at 1 ppm; I_{gas}/I_{air} = 15.7 at 5 ppm; I_{gas}/I_{air} = 19.5; and I_{gas}/I_{air} = 22.4 at 16 ppm). In Fig. 6(a), the bare SnO_2 nanotubes also show large sen-

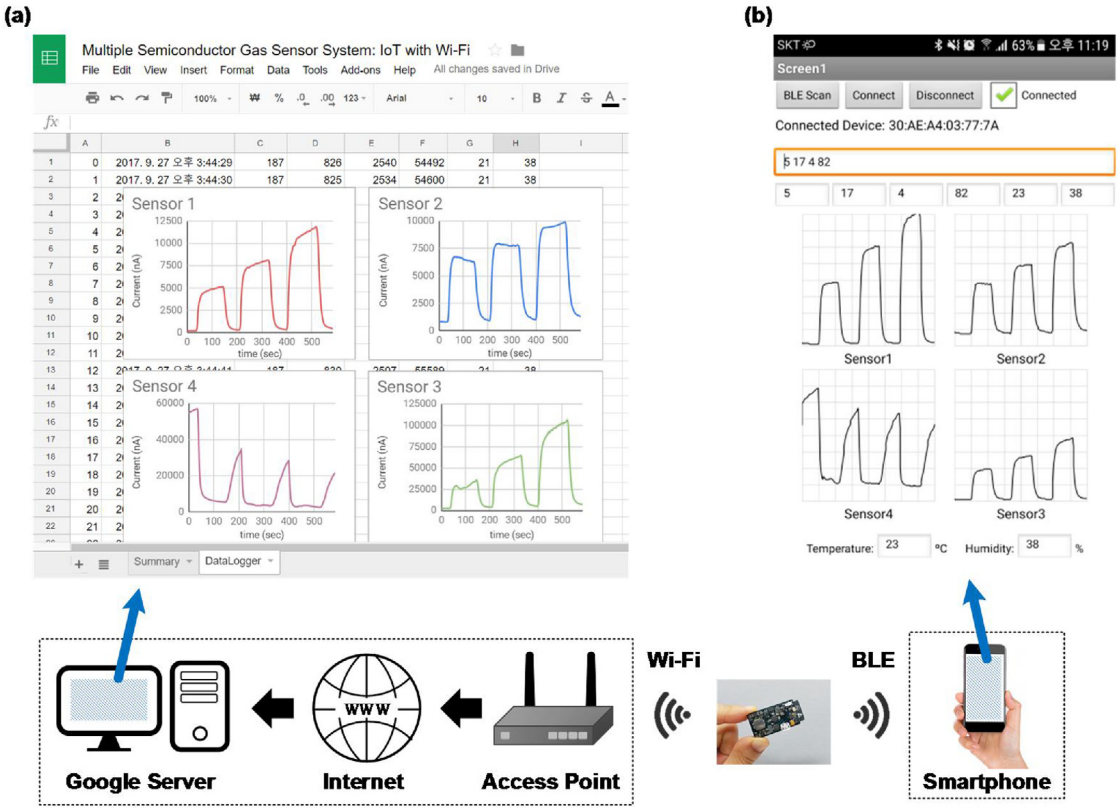

Fig. 9. Raw data transmission of multiple sensors by ESP32 through Wi-Fi and BLE: (a) Data transmission through an internet-connected access point that provides Wi-Fi. Here, the sensor data is logged into a Google Spreadsheet file and represented in the graphs. (b) Data transmission through a BLE to Android app that plots real-time graphs of the sensor data.

sitivity to H_2S gas (I_{gas}/I_{air} = 3.0 at 1 ppm; I_{gas}/I_{air} = 5.5 at 5 ppm; I_{gas}/I_{air} = 7.0; and I_{gas}/I_{air} = 8.7 at 16 ppm). Both SnO_2-based sensing materials show fast response and recovery (80% response and recovery time <20 s). On the other hand, in Fig. 6(c), bare ZnO nanowires show relatively lower sensitivity for the whole concentration range of H_2S (I_{gas}/I_{air} = 1.3 at 1 ppm; I_{gas}/I_{air} = 1.7 at 5 ppm; I_{gas}/I_{air} = 2.1; and I_{gas}/I_{air} = 2.6 at 16 ppm). In addition, in Fig. 6(d), the enhancement of sensitivity caused by Pt-catalytic effect was not clearly shown in Pt-coated ZnO nanowires (I_{gas}/I_{air} = 1.3 at 1 ppm; I_{gas}/I_{air} = 1.6 at 5 ppm; I_{gas}/I_{air} = 1.9; and I_{gas}/I_{air} = 2.1 at 16 ppm).

Since the module is specially designed for multiplexed gas sensors, it is possible to give further analysis such as principal component analysis (PCA), which is an effective measure to overcome the poor selectivity problem of semiconductor metal oxide-based gas sensors. For this analysis, sensing of H_2S and CO gases were tested because they are both reducing gases that increase the conductance of n-type semiconductor metal oxides, which makes it harder to distinguish them. In addition, considering the environmental monitoring application of this module, H_2S and CO are among the most significant target gases, causing headache, nausea, paralysis, dyspnea, or damage to nerve system when exposed to human body. Using the module, we acquired four sensors' sensitivity values. Fig. 7(a) shows different sensitivity values to these two gases and Fig. 7(b) is a PCA result acquired from the sensitivity. Even though H_2S and CO are reducing gases, sufficiently distinct distribution of the PCA points may enable the discrimination of different gases. Designed multichannel sensing module has high computing capacity by ESP32 (32-bit dual core and 80–240 MHz clock frequency) that enables relatively heavy computation. Exploiting hardware resources of the module and a remote computer that receives data, software implementation for PCA will result in the selectivity enhancement of the gas sensing system.

Our module can be readily programmed to give various operation modes, and one of them is power saving. In a limited power source condition, such as battery power, it is recommended for the whole system to be turned on and off intermittently. Since four-channel heating consumes significant amount of power, it should also be repeatedly turned on and off to reduce the power consumption. Here, the heaters should respond fast enough to give proper temperature condition to the sensors as soon as possible to save on-time. We reprogrammed the ESP32 to give a pulse heating condition to a heater in a way of changing DAC value repeatedly. Fig. 8(a) is resultant current through the heater by a pulse voltage over time, and Fig. 8(b) shows the overall response to H_2S in the pulse heating condition. Although its sensitivity and response/recovery speed are reduced compared to the continuous heating condition, the sensor still gives fair gas response and recovery/response speeds in the pulse-heating mode. This shows that our module and sensor reliably operate despite frequent sleep and wake-up repetitions.

As shown in Fig. 9, we suggest two possible scenarios of IoT applications using Wi-Fi and BLE hardware which are already equipped in ESP32. According to an open-source IoT project on the internet [15], it can be found out that ESP32 can log the sensor data into Google Spreadsheet using HTTPS Redirect technique and a published web application written in Google Script. With reference to the project, we got our sensor data logged into a Google Spreadsheet file through an internet-connected access point, and the result is shown in Fig. 9(a). For the BLE communication, we developed an Android app that plots real-time sensor graphs through MIT App Inventor, an online Android programming environment. Here, ESP32 on our module acts as a BLE server that contains sensing data and lets the clients in vicinity notice this server by doing 'advertisement'. When it is bonded to a smartphone, the data is continuously fed to the smartphone using the 'notify' property which facilitates

the transmission of a data stream. Fig. 9(b) shows that the transmitted data is properly parsed and plotted on four graphs. The domain of each axis is the same as those for the graphs in Fig. 9(a), and their scale is previously set for each line to be fully visible.

Overall circuit power consumption without heating operation is 420 mW, where communication part in ESP32 takes 330 mW (78% of total circuit power). This is rather high for portable applications where BLE is used. The current version of software framework for ESP32, still being updated, only supports combined mode of Bluetooth Classic and BLE mode yet [16], and is considered as the cause of the high power consumption. Taking into account other commercially available UART-supported BLE-only devices consume a tens of mW, we consider that there is a room for remarkable power reduction for BLE-only mode in the future framework/chip updates.

5. Conclusions

A highly portable multiple gas sensing module with semiconductor-type chemiresistive sensors has been proposed in the present work. Multiple gas sensors were integrated on a small-sized platform and put on the module. Various system demonstrations including electronics and sensors were conducted: real-time gas responses, PCA, pulse-heating, and data transmission using Wi-Fi/BLE. AFE was designed to remain high sensing accuracy over wide range variation of resistance (R_{sens}) and to control heating power to target levels even with the variation in R_{heat}. The microcontroller-RF combined SoC enabled various IoT applications including stationary and portable usage. Although the current system has power consumption issue for communication, it is expected to be resolvable by further updates of ESP32. Since this system fully integrates sensor, AFE, digital signal processing, and RF, it does not need an intermediate device and can be directly applied to IoT use. Due to its small size and high functionality, this system can be applied to various applications such as air quality monitoring in manufacturing sites, home, vehicle, etc.

Acknowledgements

This research was supported by the project titled 'Development of Management Technology for HNS Accident', funded by the Ministry of Oceans and Fisheries (Korea) and by Nano Material Technology Development Program (2015M3A7B7045518) through the National Research Foundation of Korea (NRF) funded by the Ministry of Science and ICT (Korea).

Appendix A. Supplementary data

Supplementary data associated with this article can be found, in the online version, at https://doi.org/10.1016/j.snb.2018.03.099.

References

[1] I. Cho, K. Kang, D. Yang, J. Yun, I. Park, Localized liquid-phase synthesis of porous SnO_2 nanotubes on MEMS platform for low-power, high performance gas sensors, ACS Appl. Mater. Interfaces 9 (2017) 27111–27119.
[2] K.-M. Park, T.-W. Kim, J.-H. Park, C.-O. Park, Applicability of superposition for responses of resistive sensors in diluted mixed gas environment, Sens. Actuators B-Chem. 239 (2017) 841–847.
[3] A. De Marcellis, G. Ferri, Analog Circuits and Systems for Voltage-Mode and Current-Mode Sensor Interfacing Applications, Springer, New York, 2011.
[4] A. Baschirotto, S. Capone, A. D'Amico, C. Di Natale, V. Ferragina, G. Ferri, L. Francioso, M. Grassi, N. Guerrini, P. Malcovati, E. Martinelli, P. Siciliano, A portable integrated wide-range gas sensing system with smart A/D front-end, Sens. Actuators B-Chem 130 (2008) 164–174.
[5] J.-H. Park, K.-M. Park, S. Kim, C.-O. Park, H.-J. Yoo, Three-electrode metal-oxide gas sensor system with CMOS interface IC, IEEE Sens. J. 17 (2017) 784–793.
[6] J.-H. Suh, J.-H. Park, S.-J. Kweon, H.-J. Yoo, Multiparameter sensor interface circuit with integrative baseline/offset compensation by switched-capacitor level shifting/balancing, IEEE Trans. Circuits Syst. II, Exp. Briefs 65 (2018) 316–320.
[7] S.E. Moon, N.-J. Choi, H.-K. Lee, J. Lee, W.S. Yang, Semiconductor-type MEMS gas sensor for real-time environmental monitoring applications, ETRI J. 35 (2013) 617–624.
[8] D.K. Sharma, R.S.V. Dwara, B.A. Botre, S.A. Akbar, Temperature control and readout circuit interface for Mox based NH3 gas sensor, Microsyst. Technol. 23 (2017) 1575–1583.
[9] K. Hu, V. Sivaraman, B.G. Luxan, A. Rahman, Design and evaluation of a metropolitan air pollution sensing system, IEEE Sensors J. 16 (2016).
[10] D. Kim, D. Yang, K. Kang, M. Lim, Z. Li, C. Park, I. Park, In-situ integration and surface modification of functional nanomaterials by localized hydrothermal reaction for integrated and high performance chemical sensors, Sens. Actuators B-Chem. 226 (2015) 579–588.
[11] D. Yang, M.K. Fuadi, K. Kang, D. Kim, Z. Li, I. Park, Multiplexed gas sensor based on heterogeneous metal oxide nanomaterial array enabled by localized liquid-phase reaction, ACS Appl. Mater. Interfaces 7 (2015) 10152–10161.
[12] D. Yang, D. Kim, S.H. Ko, A.P. Pisano, Z. Li, I. Park, Focused energy field (FEF) method for the localized synthesis and direct integration of 1D nanomaterials on microelectronic devices, Adv. Mater. 27 (2015) 1207–1215.
[13] D. Yang, K. Kang, D. Kim, Z. Li, I. Park, Fabrication of heterogeneous nanomaterial array by programmable heating and chemical supply within microfluidic platform, Sci. Rep. 5 (2015) 8149.
[14] C.Y. Jin, J. Yun, J. Kim, D. Yang, D.H. Kim, J.H. Ahn, K.-C. Lee, I. Park, Highly integrated synthesis of heterogeneous nanostructures on nanowire heater array, Nanoscale 6 (2014) 14428–14432.
[15] How to Post Data to Google Sheets using ESP8266, http://embedded-lab.com/blog/post-data-google-sheets-using-esp8266/. 2016.
[16] ESP32-IDF Programming Guide v2.1, http://esp-idf.readthedocs.io/en/v2.1/api-reference/bluetooth/controller_vhci.html. 2017.

Biographies

Ji-Hoon Suh received his B.S. in electrical and electronics engineering from Chung-Ang University (2013) and M.S. in electrical engineering from KAIST (2016). He is currently a researcher at KAIST. His main research interests are sensor interface circuits and embedded applications.

Incheol Cho received his B.S. and M.S. from KAIST (2015, 2017), both in mechanical engineering. He is currently a doctoral student at KAIST. His main research interests are MEMS fabrication and highly integrated gas sensor based on nanomaterials.

Kyungnam Kang received his B.S. in nanomechatronics engineering from Pusan National University (2013) and M.S. in mechanical engineering from KAIST (2015). He is currently a doctoral student at KAIST. His main research interests are nanomaterial-based sensors, MEMS fabrication and printing technologies.

Soon-Jae Kweon received his B.S. and Ph.D. from KAIST (2010, 2018) in electrical engineering. He is currently a postdoctoral researcher at KAIST. His main research interests are sensor interface circuit, bio-impedance measurement circuit, and RF systems for mobile communications.

Moonjin Lee received his B.S. (1989), M.S. (1991), and Ph.D. (1996) from Pukyong National University, all in oceanography. He has been senior and principal researcher in Korea Institute of Ocean Science and Technology (KIOST) since 1996, and an adjunct professor at the University of Science and Technology (UST), Korea since 2012. His main research interests are protection technology for hazardous and noxious substances (HNS) and real-time monitoring of physical parameters in the ocean environment.

Hyung-Joun Yoo received the B.S. degree in physics from Seoul National University, Seoul, South Korea, in 1979, and the M.S. and Ph.D. degrees in physics from the Korea Advanced Institute of Science and Technology (KAIST), Daejeon, South Korea, in 1990 and 1994, respectively. From 1979 to 1982, he was with the Agency for Defense Development. In 1983, he joined the Electronics and Telecommunications Research Institute, where he was a Director of the Advanced Technology Research Department until 1997. From 1998 to 2009, he was a Professor with the Information and Communications University. Since 2009, he has been a Professor with KAIST. His research interests include RF systems for mobile communications, reconfigurable RF integrated circuits, RF identification, and sensor read-out integrated circuits. Dr. Yoo was the recipient of the Best Paper Award of the IEEE Transactions on Industrial Electronics in 2011.

Inkyu Park received his B.S., M.S., and Ph.D. from KAIST (1998), UIUC (2003) and UC Berkeley (2007), respectively, all in mechanical engineering. He has been with the department of mechanical engineering at KAIST since 2009 as a faculty and is currently an associate professor. His research interests are nanofabrication, smart sensors, nanomaterial-based sensors and flexible & wearable electronics. He has published more than 70 international journal articles (SCI indexed) and 100 international conference proceeding papers in the area of MEMS/NANO engineering. He is a recipient of IEEE NANO Best Paper Award (2010) and HP Open Innovation Research Award (2009–2012).